06

Few-layer graphene as an additive in the fabrication of fine-grained concrete-based composites

© T.A. Koriakovtseva,[1] A.E. Dontsova,[1] A.A. Vozniakovskii,[2] E.I. Kalashnikova[2]

[1]Peter the Great Saint-Petersburg Polytechnic University,
194064 St. Petersburg, Russia
[2]Ioffe Institute,
194021 St. Petersburg, Russia
e-mail: tamusorina@mail.ru

Received March 20, 2025
Revised May 16, 2025
Accepted September 2, 2025

The study is devoted to preliminary assessments of the possibility of using few-layer graphene synthesized via self-propagating high-temperature synthesis (SHS) as an additive to fine-grained concrete in order to improve the thermal insulation properties of the resulting composite. The introduction of the graphene additive increased the stiffness and reduced the workability of the concrete mixture. Based on the test results and comparison of experimental samples with control series without additives, it was found that the addition of few-layer graphene at 5 vol.% reduces the thermal conductivity coefficient by 46.3 %, which doubles the heat storage capacity of this material compared to the original sample without compromising the complex of strength properties.

Keywords: construction materials, fine-grained concrete, graphene, few-layer graphene, three-point bending, bending, compression, thermal conductivity.

DOI: 10.61011/TP.2026.02.62880.40-25

Introduction

Concrete is one of the most widespread modern construction materials. However, modern construction industry requires new, more perfect grades of concrete. To solve this problem, researchers actively use the concept of composite materials. Combining the properties of initial matrix (concrete) and various fillers (for example, microsilica [1], aerogel [2], silicon and clay nanofractions [3], etc.), researchers are able to improve various properties of concretes significantly: increase mechanical strength, reduce brittleness, increase frost resistance, reduce water permeability or improve heat resistant properties of the final composite material [4,5].

Graphene nanostructures (GNS) are one of the most promising classes of fillers for creating concrete-based composites. Interest in GNS is driven by their record-breaking properties. For example, Young's modulus of graphene can reach up to 1 TPa [6], and its thermal conductivity is up to 5000 W/(m·K) [7]. Due to such properties, addition of even small amounts of GNS shall provide considerable growth of properties of finished composites.

Thus, in [8], it was reported that addition of 0.0208 % graphene increases the mortar strength by 12 %. But even for these materials, which are simpler than concrete, there are many problems to be solved.

One of the important problems in introducing an additive into a mixture is providing uniform nanomaterial distribution in the cement matrix [9]. Thus, in [4,10], to achieve this goal, it is proposed to use water-dispersed graphene dissolved in water mixing concrete ingredients with water. In [11], aqueous slurry of graphene was also used for producing concrete with coarse aggregate. Various forms of graphene, for example, graphene oxide [12], graphene nanoplatelets [13], functionalized graphene [14] are considered for use as additives. Researchers also face a complex task of choosing an optimum proportion for adding graphene to concrete. One of the ways of solution is creating an experimental database containing test results for concrete with a graphene additive introduced in a concrete mixture in various amounts and proportions. Detailed experiments were performed in [10,15–19]. The best increments of mechanical strength of concrete in [15] were achieved by introducing 0.03 % and 0.09 % of graphene oxide by the mass of cement together with 5 % or 9 % of microsilica. In [11], the best result was shown by compounds containing 0.07 % of graphene. A wide review of studies concerning the change of concrete properties via graphene introduction is given in [12,20]. In [21], combined effect of graphene oxide and steel fiber on resultant concrete strength was estimated, and possibility of combining graphene with other known additives to concrete was also shown. Generally it can be concluded that, though graphene is currently an expensive additive, introducing it in a concrete mixture in various forms has a positive effect on the end-use properties of concrete composite. Moreover, possibility to add graphene to concrete opens a prospect of creating concrete with a built-in condition monitoring function [22]. There is currently a set of unexplored questions concerning graphene-containing concrete, including: long-term influence of the additive on concrete, mode of interaction between graphene particles

Table 1. Composition of 1 l of concrete mixture

Type of mixture	Portland cement M400, g	Quartz sand $0-0.63$ mm, g	Plasticizer, g	Water, g	Additive, g
Reference	687.0 ± 0.2	1253.0 ± 0.2	7.00 ± 0.1	253.0 ± 0.1	0
FLG (5 vol.%) (G1–G3)	652.6 ± 0.2	1190.3 ± 0.2	6.65 ± 0.1	240.4 ± 0.1	51.2 ± 0.1
FLG (10 vol.%) (G4–G6)	618.2 ± 0.2	1127.6 ± 0.2	6.50 ± 0.1	227.7 ± 0.1	102.4 ± 0.1

and cement in the mixture, optimum amount of additive and prospects of using graphene-containing concrete on a commercial scale [23].

However, despite the fact that GNS provide significant increase in critical operating properties of concretes, they haven't been applied in real practice yet for a number of reasons. The key reason for not using GNS in real industry is imperfection of synthesis techniques both in terms of „top-down" [24] approach and „bottom-up" approach [25], preventing from synthesizing large amounts of a high quality material at a reasonable cost.

The previous studies developed a new synthesis technique for few-layer graphene (FLG, maximum 5 layers [ISO/TS 21356-1:2021]) in the self-propagating high-temperature synthesis conditions (SHS) to synthesize large amounts of low-cost material [26] free of the Stone-Wales defects [27]. It was found that the synthesized FLG provided a considerable increase in a set of strength and thermal-physical properties of polymer composites on the basis of photopolymer resins [28].

The aim of this work is to study experimentally the efficiency of FLG synthesized in SHS conditions as an additive for increasing heat-storage capacity of fine-grained concretes.

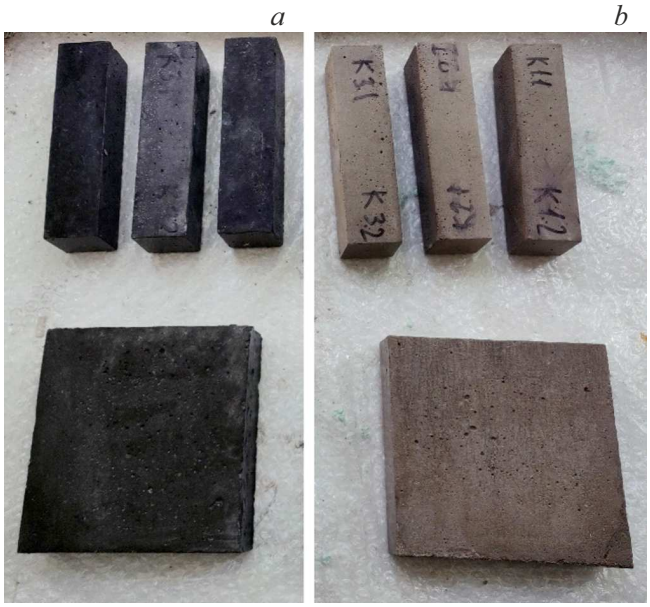

Figure 1. View of fine-grained concrete composite samples with 5 vol.% FLG (*a*) and reference samples (*b*) for three-point bending test (prisms) and thermal conductivity coefficient (plate) measurements.

1. Materials and methods

1.1. Synthesis of fine-grained concrete composite materials

Fine-grained concrete was used as the basis for preparing composites. Quartz sand with a grain size of $0-0.63$ mm was used as filler.

FLG was used as a modifying additive (max. 5 layers in accordance with the international standard [29]) synthesized from microcrystalline cellulose (AR grade, India) in SHS conditions. For details of the synthesis technique and material properties, see [30]. The essence of the technique is in formation of graphene planes from carbon backbones originating from various biopolymer molecules (microcrystalline cellulose in this case) exposed to a high-temperature SHS wave [26].

Samples were prepared via step-by-step addition of ingredients into a mixer. All dry ingredients were mixed first; cement, sand and additive, then water with plasticizer were added gradually. Molds filled with the mixture were subjected to vibrations on a shaking table during 120 s to remove air bubbles from the mixture. After concrete pouring, the samples were stored in a wet environment during 28 days to gain in strength. Samples were tested at 28 days.

Three $160 \times 40 \times 40$ mm prisms were made from each type of mixtures for three-point bending and compressive strength test, and $15 \times 15 \times 3.5$ cm samples were made for thermal conductivity measurements. Water-cement ratio remained constant for all samples. Compositions of the fine-grained concrete reference sample and fine-grained concrete composites are shown in Table 1.

The view of samples is shown in Figure 1.

1.2. Techniques

Mean linear dimensions of FLG particles were measured using the laser diffraction technique (Mastersizer 2000,

Malverin, UK). For particle dispersion measurement, aqueous suspensions of FLG (concentration of 0.1 mass%) were prepared using ultrasonic bath treatment (frequency of 22 kHz). Specific surface area and porosity of FLG were measured by low-temperature nitrogen sorption using the Brunauer–Emmett–Teller method (BET) and statistical thickness method (STSA) on the Sorbi-MS meter (Russia). Before measurement, the sample was subjected to sample preparation by vacuum annealing at 250 ° during 2 h.

Concrete samples were tested on the following machines: MII-100 (USSR) three-point bending test machine and 50 ton hydraulic press (USSR) for compression test.

Brinell hardness of the synthesized samples was measured on the ITB-3000-AM (Russia) Brinell hardness tester. Indentation diameter was measured using a digital camera and manufacturer's specialized software.

Thermal conductivity coefficient and thermal resistance of samples were measured by the continuous heat flux method using the ITS-1 meter (Russia). Maximum relative measurement error of the ITS-1 meter is 5 %.

2. Findings and discussion

Electron microscopy image of FLG particles is shown in Figure 2.

Figure 2 shows that FLG particles in powder are in the form of aggregates, whose size can reach several tens of microns. To evaluate the real linear size, dispersion was investigated using the laser diffraction method as shown in Figure 3.

As shown in Figure 3, though the sample contains FLG particles, whose linear sizes reach tens and hundreds of microns (Figure 3, *a*), percentage of such particles is low and most of FLG particles ($\sim 50\,\%$) have linear sizes within $1.2-1.4\,\mu$m.

Table 2 shows the specific surface area measurements of FLG particles.

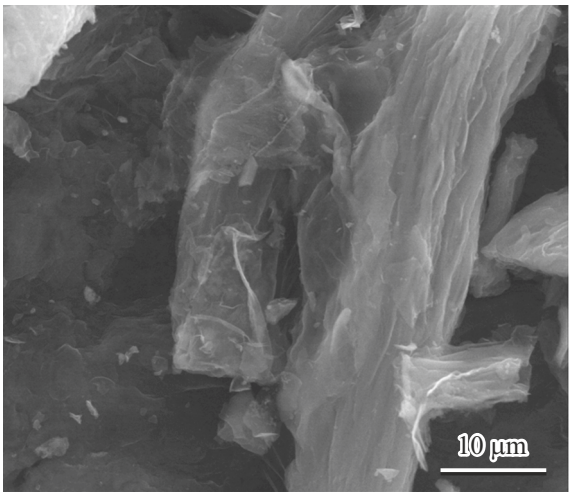

Figure 2. Electron microscopy image of FLG particles.

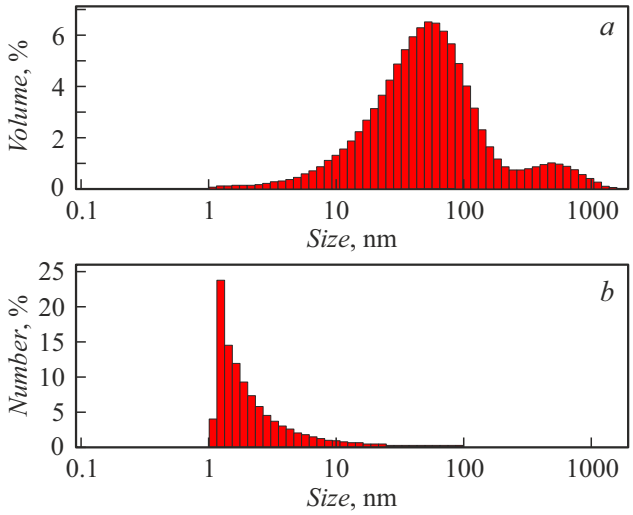

Figure 3. FLG particle measurements: *a* — size distribution of FLG particle volume; *b* — size distribution of the number of FLG particles.

FLG specific surface area measured by the STSA method is relatively small and is equal to 86 m^2/g. However, the total specific surface area of the sample is much larger and is equal to 320 m^2/g due to the partial contribution of micropores, whose volume was measured using the BET method.

FLG additive to the concrete mixture increased the mixture hardness and reduced the mixture spreadability. The concrete mixture with the FLG additive was the least workable one among all mixtures and had low flowability. Such effects produced by adding graphene to a concrete mix were also noted by other researchers [12]. Figure 4 shows cross-section images of the initial concrete sample and concrete sample with FLG additive.

As shown in Figure 4, *a*, cross-section of the initial concrete sample has $100-200\,\mu$m honeycombs, while the sample with FLG has no such honeycombs.

Strength properties of concretes play the key role in concrete applications. Figure 5 and 6 show three-point bending and compressive strength measurements, respectively.

As shown in Figure 5, introduction of FLG doesn't lead to any significant change (change within the method error) in bending strength. However, with 10 vol. % FL, the compressive strength decreases by 18 % compared with the reference sample (Figure 6).

Figure 7 shows strength measurements of the synthesized samples.

As shown in Figure 7, unlike the compressive strength and three-point bending strength, addition of 5 vol. % FLG provided an increase in the composite hardness by 44 %. However, further increase in the FLG concentration (up to 10 vol. %) didn't result in further hardness growth.

Summarizing the strength data for initial concrete and FLG composite samples with the findings for sample cross-sections, it is suggested that addition of RMSD reduces the concentration of structural defects in the composite

Table 2. FLG specific surface area and porosity measurements

Specific surface area, STSA, m^2/g	Specific surface area, method BET method, m^2/g	Pore volume, cm^3/g	Micropore volume, cm^3/g
86 ± 4	320 ± 4	0.190 ± 0.005	0.107 ± 0.003

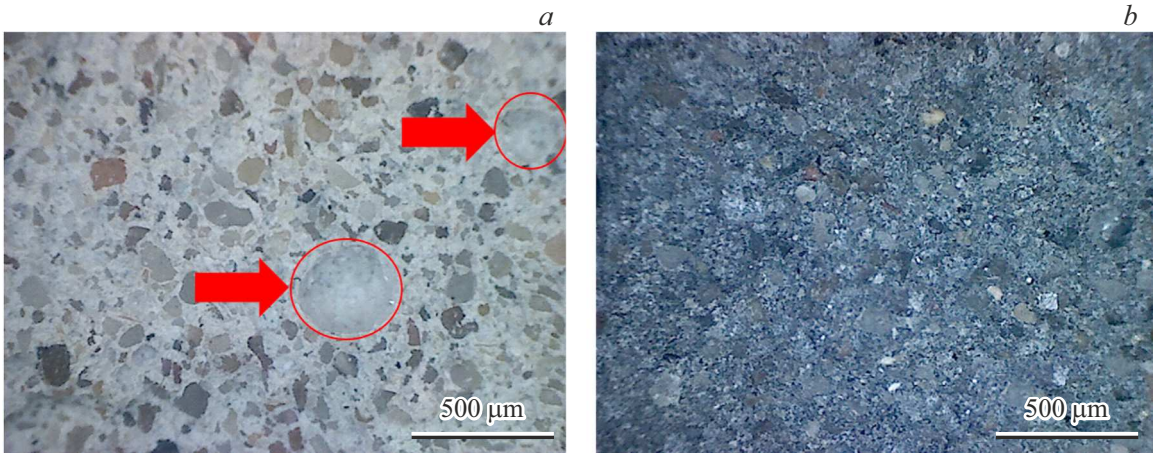

Figure 4. Cross-sections of initial concrete (a) and 10 vol.% FLG (b). Red arrows show voids.

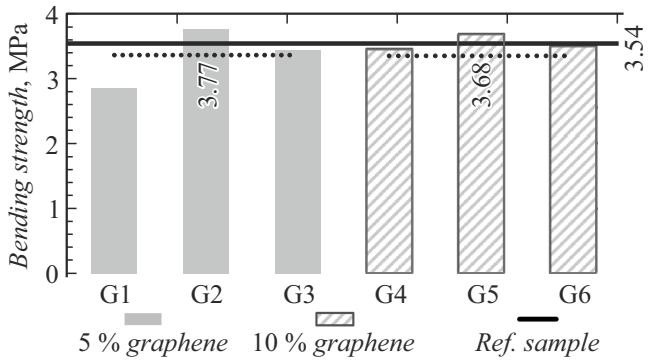

Figure 5. Three-point bending strength measurements of composite samples depending on the FLG concentration.

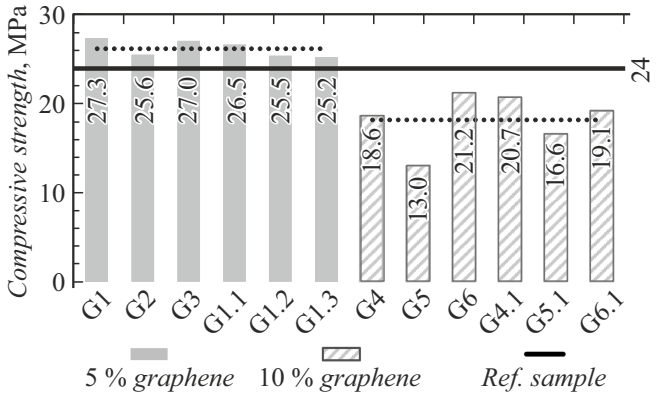

Figure 6. Compressive strength measurements of composite samples depending on the FLG concentration.

(pores, honeycombs, etc.), providing the growth of strength properties.

Figure 8 shows the thermal conductivity and thermal resistance measurements of the synthesized samples at 25 °C.

As shown in Figure 8, introduction of 5 vol.% FLG results in approximately twofold reduction of thermal conductivity compared with the reference sample. However, as the FLG percentage increases to 10%, the gap in thermal conductivity compared with the reference sample decreases and is already 30%.

The findings were interpreted by calculations using several mathematical models.

There is a set of models for predicting composite conductivity on the basis of properties of nanoparticles (NPs) and base ingredient to take into account their proportion in the compound [31].

Maxwell model [32] represented by equation (1) is empirical and features good accuracy and simplicity for spherical particles with low concentrations. Being one of the first in its class, it is widely used as a basis for other models where additional parameters or corrections are added.

$$KnfMaxwell = Kbf\left(\frac{Knp + 2Kbf + 2\varphi(Knp - Kbf)}{Knp + 2Kbf - 2\varphi(Knp - Kbf)}\right). \quad (1)$$

In this equation and in the following equations, Knf corresponds to thermal conductivity of the composite, Knp corresponds to thermal conductivity of NPs, Kbf corresponds

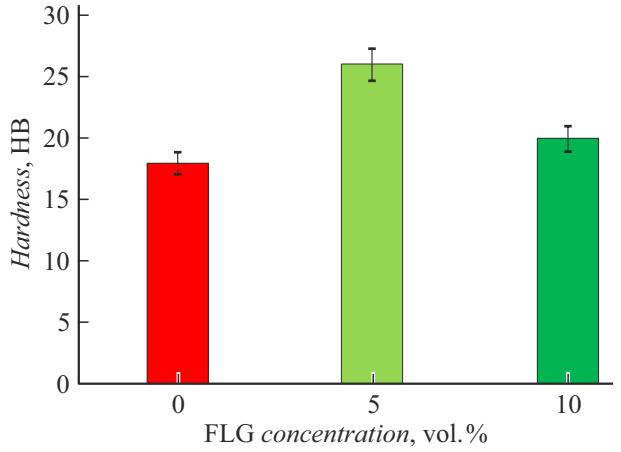

Figure 7. Brinell strength measurements of composite samples depending on the FLG concentration.

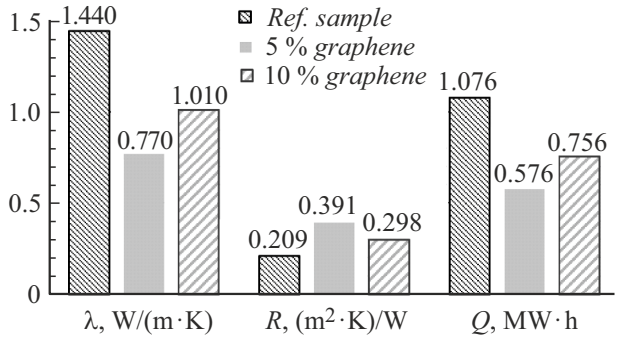

Figure 8. Thermal-physical property measurements of samples depending on the FLG concentration.

to thermal conductivity of the base ingredient (cement), φ is the concentration of NPs. Equation (2) presented by Crosser [33] is based on the same concept, however, it also includes a parameter related to the particle shape. Thus, the shape factor n is defined by particle sphericity in such a way as shown in equation (3), particle sphericity depends on the particle shape, for example, for a sphere $\omega = 3$, and for a cylinder $\omega = 0.5$.

$$KnfH\&C = Kbf \times \left(\frac{Knp+(n-1)Kbf-\varphi(n-1)(Kbf-Knp)}{Knp+(n-1)Kbf+\varphi(Kbf-Knp)}\right), \quad (2)$$

$$n = \frac{3}{\omega}. \quad (3)$$

Hashin-Shtrikman model represented by equation (4) was used to additionally confirm the reliability of experimental Knf data, which usually imply that nanosheets are adequately dispersed in the matrix [34]:

$$KnfH\&S = Knp\left(1+\frac{3+(1-\varphi)(Knp-Kbf)}{3Knp-(Knp-Kbf)}\right). \quad (4)$$

Note that, when the thermal conductivity of the base ingredient (cement) and the volume fractions of the base ingredient and nanoparticles (NP) are known, then the real thermal conductivity of nanoparticles is unknown in advance because it depends on many parameters: degree of aggregation, defects, etc. In Figure 9, the experimental thermal conductivity of the composite with 5 vol.% FLG at 20 °C is compared with the Maxwell, Hamilton–Crosser and Hashin–Shtrikman model data depending on the expected thermal conductivity of NPs.

Figure 9 shows that the Maxwell model, where the nanoparticle shape was taken as spherical, and the Hamilton–Crosser model, where the nanoparticle shape was taken as cylindrical, almost coincide with each other and provide poor fit between the calculated thermal conductivity of the composite and the experimental data. While the Hashin–Shtrikman model, where the particle shape is taken as close to a sheet, demonstrates another mode of dependence compared with two previous models and provides satisfactory fit between the calculated thermal conductivity of the composite and experimental data with thermal conductivity of nanoparticles of only 0.35 W/(m·K).

Satisfactory fit of the Hashin–Shtrikman model data suggests that FLG particles are distributed in the water volume in the form of aggregates and their shape is close to a sheet. Thermal conductivity of FLG fillers can be estimated as 0.4 W/(m·K).

Figure 10 compares the experimental thermal conductivity of the composite with FLG vol. 10 % at 20 °C with the Hashin–Shtrikman model data depending on the expected thermal conductivity of NPs.

Figure 10 shows that the Hashin–Shtrikman model provides satisfactory fit between the calculated thermal

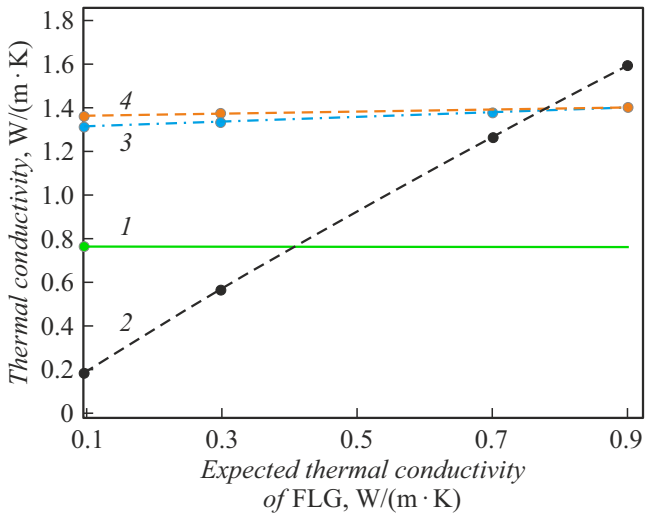

Figure 9. Thermal conductivities of the composite (cement) with FLG concentration of 5 vol.% at 20 °C calculated using various models depending on the expected thermal conductivity of NPs. *1* — experimentally measured thermal conductivity; *2* — Hashin–Shtrikman model calculation; *3* — Maxwell model calculation; *4* — Hamilton and Crosser model calculation.

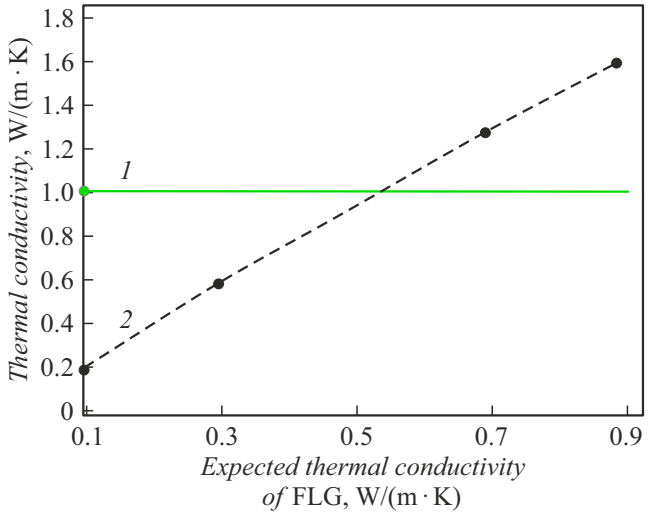

Figure 10. Thermal conductivities of the composite (cement) with FLG concentration of 10 vol.% at 20 °C calculated using various models depending on the expected thermal conductivity of NPs. *1* — experimentally measured thermal conductivity; *2* — Hashin–Shtrikman model calculation.

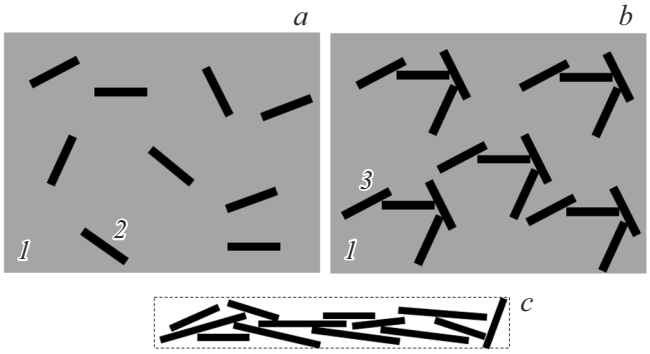

Figure 11. Structure model of the synthesized composites: *a* — 5 vol.% FLG; *b* — 10 vol.% FLG; *c* — structure of the FLG particle aggregate. *1* — concrete matrix; *2* — FLG particle aggregate; *3* — 2-nd order FLG aggregates (heat bridges).

conductivity of the composite and the experimental data with the thermal conductivity of nanoparticles of only 0.55 W/(m·K). Note that such thermal conductivity of FLG (0.4–0.55 W/(m·K)) is much lower than that of individual graphene sheets (5000 W/(m·K)) [6].

Since with addition of FLG the thermal conductivity of the finished composite decreases considerably, this is indicative of FLG distribution in the form of aggregates, rather than in the form of individual particles. Considering that the experimentally measured thermal conductivity of the composite with 5 vol.% FLG coincides only with the Hashin–Shtrikman model data, where filler particles are assumed as having a cylindrical structure, it is suggested that FLG aggregates in composites also have a cylindrical structure. Thermal conductivity calculations for the composite with 10 vol.% FLG show that the thermal conductivity of FLG aggregates grows as the volume fraction of FLG in the fine-grained concrete increases. As the FLG fraction increases, FLG aggregates presumably form chains in the concrete matrix and these chains serve as bridges for more effective heat transfer.

Summarizing the data for the set of strength and thermal-physical properties of the synthesized composites, the structure of these composites was proposed and is shown in Figure 11.

Thermal properties shall be investigated to create energy-efficient materials. Modern design and advanced technology allow engineers to fulfil all building heat insulation and energy efficiency requirements [35].

There are different solutions designed to improve building energy efficiency: various ventilated facade configurations [36], development of wall insulation thickness calculation methods taking into account temperature and humidity conditions [37,38].

The wall heat insulation increase effect is provided by reducing the heat loss through building facades and thermal protection enclosure as a whole to decrease heat energy consumption; by increasing indoor thermal comfort by means of decreasing the radiative and convective heat exchange on the inner surface of wall; and by reducing environmental pollution via greenhouse gas emission reduction [39].

Energy efficiency of the synthesized samples was identified by calculating the amount of heat Q, [MW·h]) lost by a building through its 300 mm concrete walling throughout the heating season using the following equation:

$$Q = \frac{S \cdot \Delta t \cdot z_{heating\ season}}{R_o}, \tag{5}$$

where S — is the wall area set to 1 m^2; Δt — is the difference of indoor and outdoor temperatures,

$$\Delta t = 20 - (-24) = 44\,\text{K}, \tag{6}$$

$z_{heating\ season} = 5112$ h — is the heating season duration, R_o — thermal resistance, [(m^2·K)/W].

The calculation results are shown in Figure 8. As shown in the figure, 5 vol.% FLG provides a twofold reduction of external heat energy loss by a building structure

Conclusion

FLG synthesized in SHS conditions and used in a concentration up to 10 vol.% has shown significant benefits of using this material as an additive to concrete-based composites. FLG provided significant (twofold) reduction of thermal conductivity of the synthesized samples and increase in Brinell hardness by 44% compared with the reference sample without degrading the set of strength properties (compressive strength and three-point bending strength). By comparing the thermal conductivity measurements of composites with the model calculations, it

has been found that FLG particles (with 5 vol. %) are distributed in the form of aggregates resulting in thermal conductivity reduction of the finished product. However, with further increase in the filler fraction, FLG aggregates form heat bridges leading to thermal conductivity growth. Thermal conductivity calculations have shown that, due to low thermal conductivity of composites, their heat-storage capacity shall be approximately twice as high as that of the reference sample. Calculations using the mathematical thermal conductivity models have shown that as the FLG fraction in a composite volume increases, thermal conductivity of FLG aggregates increases from 0.35 to 0.55 W/(m·K). It is suggested that as the FLG fraction increases, the size of FLG aggregates, which serve as heat conducting chains in the concrete matrix, increases.

The obtained data will be used as the basis for future work on investigating the effect of low (< 5 vol. %) FLG concentrations on the properties of concrete-based composites to improve a set of strength properties.

Funding

The study was carried out with financial support provided under the state order by the Ioffe Institute (project FFUG-2024-0019 „Functional carbon nanostructured materials“).

Conflict of interest

The authors declare no conflict of interest.

References

[1] A. Beskopylny, S.A. Stel'makh, E.M. Shcherban', L.R. Mailyan, B. Meskhi. J. Build. Eng., **51**, 104235 (2022). doi.org/10.1016/j.jobe.2022.104235
[2] T.A. Koriakovtseva, A.E. Dontsova, D.V. Nemova. Buildings, **14** (4), 1034 (2024). doi.org/10.3390/buildings14041034
[3] M.M. Mokhtar, M. Morsy, N.A. Taha, E.M. Ahmed. Constr. Build. Mater., **320**, 125537 (2022). doi.org/10.1016/j.conbuildmat.2021.125537
[4] D. Dimov, I. Amit, O. Gorrie, M.D. Barnes, N.J. Townsend, A.I.S. Neves, F. Withers, S. Russo, M.F. Craciun. Adv. Funct. Mater., **28** (23), 1705183 (2018). doi.org/10.1002/adfm.201705183
[5] J.-J. Park, S. Kim, W. Shin, H.-J. Choi, G.-J. Park, D.-Y. Yoo. Materials (Basel), **13** (8), 1828 (2020). doi.org/10.3390/ma13081828
[6] A.A. Balandin, S. Ghosh, W. Bao, I. Calizo, D. Teweldebrhan, F. Miao, Ch. Ning Lau. Nano Lett., **8** (3), 902 (2008). doi.org/10.1021/nl0731872
[7] Ch. Lee, X. Wei, J.W. Kysar, J. Honey. Science, **321** (5887), 385 (2008). doi.org/10.1126/science.1157996
[8] M. Ucak-Astarlioglu. *Graphene in cementitious materials* (Engineer Research and Development Center (U.S.), 2023), doi.org/10.21079/11681/48033
[9] M.Goisis. Tsement i ego primenenie *5–1*, 108 (2020) (in Russian).
[10] S.P. Dalal, P. Dalal. Constr. Build. Mater., **276**, 122236 (2021). doi.org/10.1016/j.conbuildmat.2020.122236.
[11] T.A.Potes, S.N.Leonovich. *Beton, modofotsirovannyi grafenom*. Arkhitekturno-stroitelny kompleks: problemy, perspektivy, innovatsii: elektronny sbornik statey III Mezhdunarodnoi nauchnoi konferentsii (Novopolotsk: Polotskii gos. un-t, 2021), s. 147–150. (in Russian) https://elib.psu.by/handle/123456789/28187
[12] P.K. Akarsh, D. Shrinidhi, Sh. Marathe, A.K. Bhat. Mater. Today Proc., **60**. 234 (2022). doi.org/10.1016/j.matpr.2021.12.510
[13] Z. Jiang, O. Sevim, O.E. Ozbulut. Constr. Build. Mater., **30**, 124472 (2021). doi.org/10.1016/j.conbuildmat.2021.124472
[14] B.A. Salami, F. Mukhtar, S.A. Ganiyu, S. Adekunle, T.A. Saleh. Constr. Build. Mater., **396**, 132296 (2023). doi.org/10.1016/j.conbuildmat.2023.132296
[15] M.M. Rashwan, M.F.M. Fahmy, A. Abdullah, M. Hesham. JES. J. Eng. Sci., **48** (1), 32 (2020). doi.org/10.21608/jesaun.2020.109052
[16] S.C. Devi, R.A. Khan. J. Build. Eng., **27**, 101007 (2020). doi.org/10.1016/j.jobe.2019.101007
[17] G.D. Fedorova, A.P. Scryabin, G.N. Alexandrov. Stroit. Mater., **767** (1–2), 16 (2019). doi.org/10.31659/0585-430X-2019-767-1-2-16-22
[18] A. Mashhadani, V. Pershin. Adv. Mater. Technol., **2** (18), 046 (2020). doi.org/10.17277/amt.2020.02.pp.046-056
[19] K.A. Al-Shiblavi, V.F. Pershin, T.V. Pasko. Vektor Nauk. Tol'yattinskogo Gos. Univ., **4**, 6 (2018). doi.org/10.18323/2073-5073-2018-4-6-11
[20] A.H. Alateah. Case Stud. Constr. Mater., **19**, e02653 (2023). doi.org/10.1016/j.cscm.2023.e02653
[21] O. Zaid, S.R.Z. Hashmi, F. Aslam, Z. Ul Abedin, A. Ullah. Diam. Relat. Mater., **124**, 108883 (2022). doi.org/10.1016/j.diamond.2022.108883
[22] W. Li, F. Qu, W. Dong, G. Mishra, S.P. Shah. Constr. Build. Mater., **331**, 127284 (2022). doi.org/10.1016/j.conbuildmat.2022.127284
[23] H. Zeng, Sh. Qu, Y. Tian, Y. Hu, Y. Li. J. Build. Eng., **69**, 106192 (2023). doi.org/10.1016/j.jobe.2023.106192
[24] N. Kumar, R. Salehiyan, V. Chauke, O.J Botlhoko, K. Setshedi, M. Scriba, M. Masukume, S.S. Ray. Flat Chem., **27**, 100224 (2021). doi.org/10.1016/j.flatc.2021.100224
[25] A. Gutiérrez-Cruz, A.R. Ruiz-Hernández, J.F. Vega-Clemente, D.G. Luna-Gazcón, J. Campos-Delgado. J. Mater. Sci., **57** (31), 14543 (2022). doi.org/10.1007/s10853-022-07514-z
[26] A. Voznyakovskii, A. Vozniakovskii, S. Kidalov. Fullerenes, Nanotub. Carbon Nanostructures, **30** (1), 59 (2022). doi.org/10.1080/1536383X.2021.1993831
[27] A. Voznyakovskii, A. Neverovskaya, A. Vozniakovskii, S. Kidalov. Nanomaterials, **12** (5), 883 (2022). doi.org/10.3390/nano12050883
[28] S. Kidalov, A. Voznyakovskii, A. Voznyakovskii, S. Titova, Y. Auchynnikau. Materials (Basel), **16** (3), 1157 (2023). doi.org/10.3390/ma16031157
[29] ISO/TS 21356-1:2021 *Nanotechnologies — Structural characterization of graphene. Part 1: Graphene from powders and dispersions*
[30] A. Voznyakovskii, A. Vozniakovskii, S. Kidalov. Nanomaterials, **12** (4), 657 (2022). doi.org/10.3390/nano12040657
[31] P.K. Das. J. Mol. Liq., **240**, 420 (2017). doi.org/10.1016/j.molliq.2017.05.071
[32] J.C. Maxwell. *A Treatise on Electricity and Magnetism* (Cambridge University Press, Cambridge: 2010), 484 p.
[33] B. Lamas, B. Abreu, A. Fonseca, N. Martins, M. Oliveira. Int. J. Therm. Sci., **78**, 65 (2014). doi.org/10.1016/j.ijthermalsci.2013.11.017

[34] Choi S.U.S. etc. Appl. Phys. Lett., **79** (14), 2252 (2001). doi.org/10.1063/1.1408272.
[35] E. Gumerova, O. Gamayunova, L. Shilova. MATEC Web Conf., **106**, 06020 (2017). doi.org/10.1051/matecconf/201710606020
[36] M. Petrichenko, S.A. Subbotina, F.F. Khairutdinova, E. Reich, D.V. Nemova, V.Ya. Olshevskiy, V. Sergeev. Mag. Civ. Eng., **73** (5), 40 (2017). doi.org/10.18720/MCE.73.4
[37] K.P.Zubareva, M.I.Rynkovskaya. Perspektivy nauki, **1**, 99 (2023). (in Russian)
[38] V.G. Gagarin, V.K. Akhmetov, K.P. Zubarev. IOP Conf. Ser. Mater. Sci. Eng., **918** (1), 012113 (2020). doi.org/10.1088/1757-899X/918/1/012113
[39] S.V. Kornienko. Vestnik Volgogradskogo gos. arkhitekturno-stroitelnogo un-ta. Seriya Stroitelstvo i arkhitektura, **49** (68), 167 (2017).

Translated by E.Ilyinskaya